Retinal Topography of Myopic Eyes: A Spectral-Domain Optical Coherence Tomography Study

In Kyung Oh,[1] Jaeryung Oh,[2] Kyung-Sook Yang,[3] Kyung Ho Lee,[2] Seong-Woo Kim,[2] and Kuhl Huh[2]

[1]Department of Ophthalmology, Wonkwang University Sanbon Hospital, Gyeonggi-do, Korea
[2]Department of Ophthalmology, Korea University College of Medicine, Seoul, Korea
[3]Department of Biostatistics, Korea University College of Medicine, Seoul, Korea

Correspondence: Jaeryung Oh, Department of Ophthalmology, Korea University College of Medicine, 126-1 Anam-dong 5-ga, Sungbuk-gu, Seoul, 136-705, South Korea; ojr4991@korea.ac.kr.

Submitted: March 1, 2014
Accepted: June 1, 2014

Citation: Oh IK, Oh J, Yang K-S, Lee KH, Kim S-W, Huh K. Retinal topography of myopic eyes: a spectral-domain optical coherence tomography study. *Invest Ophthalmol Vis Sci*. 2014;55:4313–4319. DOI:10.1167/iovs.14-14277

Purpose. The purpose of this study was to investigate topographic characteristics of the retina in myopic eyes.

Methods. We reviewed spectral-domain optical coherence tomography (SD-OCT) images of patients with myopia retrospectively. Retinal topography (RT) was defined as the topography of the retinal pigment epithelium layers. Retinal topographies were classified into several types, and the distribution and characteristics of each type were assessed in eyes with varying degrees of axial length (AL).

Results. A total of 167 subjects with myopia were included in this study. Seventy eyes (41.9%) were classified as regular (R) type, 48 (28.7%) were wave (W) type, 32 (19.2%) were band (B) type, and 17 (10.2%) were pond (P) type. The distribution of these types varied significantly among eyes with different degrees of AL ($P < 0.001$); R-type was predominant in eyes with 24 mm less than or equal to AL less than 26 mm, and P-type in eyes with AL greater than or equal to 28 mm. The retina sloped away from the cornea more frequently on the nasal side than it did on the temporal side or in between the nasal and the temporal sides, with the exception of the P-type RT. Topography of the central zone was frequently slanted, except in B-type eyes. The difference between the refractive and corneal astigmatism of eyes with P-type RT was greater than that of B-type eyes ($P = 0.002$).

Conclusions. Retinal topography varies according to the degree of AL. This variation in RT may originate from the differences between healthy eyes and highly myopic eyes, and may be related to the optical characteristics of the eye.

Keywords: myopia, optical coherence tomography, topography

Myopia is a common type of refraction error. Various changes in ocular configuration may occur in myopic eyes at the level of the cornea, lens, and most commonly the posterior segment. The presence of a staphyloma is a characteristic pathologic feature of myopia.[1] Recently, Moriyama and associates[2] showed that highly myopic eyes were not simply elongated, but instead exhibited areas of out-pouching, particularly in the posterior pole of the eye. Ohno-Matsui et al.[3] also reported that the curvature of the retinal pigment epithelium (RPE) in eyes with a high degree of myopia was different from those with emmetropia. Finally, Gaucher et al.[4] described a dome-shaped macula in highly myopic eyes, and suggested that the retinas of myopic eyes were more complicated and variable in structure.

In addition to other structures, the photoreceptor layers are the main location at which light rays should be focused.[5–8] Light rays are refracted by the cornea and converge onto the lens, where they are further refracted and focused onto the photoreceptors.[9–13] Therefore, the regularity of the photoreceptor layers may be essential for perceiving high quality images,[14,15] and deformation or distortion of the three-dimensional (3D) arrays of photoreceptors may induce image distortion and blurring.[16–18] The topography of retinal photoreceptor arrays are parallel to that of the RPE in healthy eyes. Therefore, RPE topography could represent photoreceptor topography in eyes without subretinal abnormalities. In addition to tomographic changes, advances in optical coherence tomography (OCT) technology have helped to provide information on topographic changes of the cornea and retina.[19–21] While tomographic variation of the retina in eyes with a high degree of myopia has been studied, topographic regularity of photoreceptors and the RPE has not been widely investigated in eyes with mild to moderate myopia.

Similar to previous studies that have examined the topographic characteristics of the cornea and lens,[22–24] investigation of photoreceptor and RPE topography would be helpful for understanding the pathophysiology of myopia. We hypothesized that the topographic characteristics of retinal photoreceptor arrays in eyes with mild myopia would be different from those in eyes with high myopia and that the differences would be related with optical measurement such as refractive astigmatism. Therefore, we characterized the topography of the retina using spectral-domain OCT (SD-OCT) and investigated the relationship between the characteristics

Copyright 2014 The Association for Research in Vision and Ophthalmology, Inc.

Downloaded from iovs.arvojournals.org on 06/26/2022

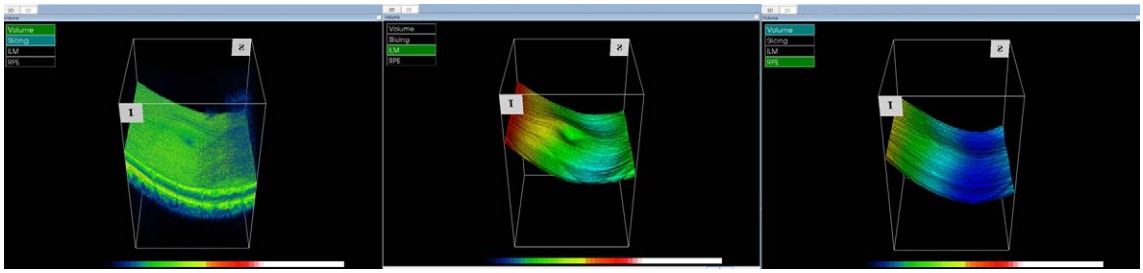

FIGURE 1. Volume scan (*left*) and layer image map (*middle*, *right*) generated using SD-OCT. The topographic layer image map of the internal limiting membrane (*middle*) and RPE (*right*) represents the inner and outer retinal topography, respectively. The rainbow pseudocolors in the topographic layer image represent height from the coronal plane of the eye, with *blue* indicating low height and *red* indicating high height.

and optical biometry in eyes with low to high degrees of myopia.

METHODS

This study was approved by the institutional review board at Korea University. The study protocol and methods of data collection were in adherence with the tenets of the Declaration of Helsinki.

For this observational case study, we examined OCT images from the SD-OCT database (3D OCT-1000 Mark II; Topcon Corp., Tokyo, Japan) at the Korea University Medical Center that were obtained between July 2009 and November 2012 retrospectively. Patients who were diagnosed with myopia of less than 0 diopters (D) of SE and an axial length (AL) of greater than or equal to 24 mm were included in this study. Eyes with pre-existing ocular disease or a history of ocular surgery other than cataract surgery were excluded. When both eyes of a subject were included, right eye was selected from each subject for analysis. The original refractive errors were used for eyes that had previously undergone cataract surgery. All patients underwent biomicroscopic and biometric examinations as well as SD-OCT. Best-corrected visual acuity (BCVA) was measured using a Snellen chart. Refractive error was measured using an automated refractor (RK-F1; Canon Inc., Tochigi, Japan). Keratometric values (K), AL, and anterior chamber depth (ACD) measured using partial coherence interferometer (IOLMaster; Carl Zeiss Meditec, Dublin, CA, USA) were also obtained. The horizontal K value was defined as the K value of the axis ranging from 0° to 45° and 136° to 180°, and the vertical K value was defined as the K value of the axis ranging from 46° to 135°. Corneal astigmatisms were calculated using the difference between flat and steep K values, and the axis of the flat K value was recorded. The axis difference between the refractive astigmatism and the corneal astigmatism was obtained as previously described.[25] Anterior chamber depth was not analyzed in eyes with a history of cataract surgery or peripheral iridotomy, or in patients whose measurements were obtained after pharmacologic mydriasis.

Retinal Topography in SD-OCT

The SD-OCT device (3D OCT-1000 Mark II, Topcon Corp., Tokyo, Japan) used in this study had a wavelength of 840 nm, a horizontal resolution of less than or equal to 20 μm, and an axial resolution of up to 5 μm. Its imaging speed was 27,000 axial scans per second. Patients underwent SD-OCT evaluations using 3D scanning protocols with 128 B-scans (512 A-scans per B-scan) of a 6 mm × 6 mm area and line scanning protocols with an average of 50 B-scans (1024 A-scans per B-scan) with a 6-mm length. Patients were sat straight in their chair with their chin firmly in the chinrest and their forehead against the headrest. The SD-OCT used a protocol to reconstruct maps of the retinal layers including the internal limiting membrane (ILM) and RPE. Each mapped layer contained information regarding the topographic data as depicted by pseudocolor values. In SD-OCT images, ILM, and RPE topography may represent inner and outer RT, respectively (Fig. 1). In this study, RT was defined as topography of the external boundary of the retinal layers on SD-OCT scans, which was determined on pseudocolor coded topographic maps of the RPE.

Classification of Retinal Topography Type

Unlike corneal topography, there is currently no established method for classifying RT type.[22,23,26] As a result, a new classification system was devised by one of our investigators (JO). Pseudocolors on topographic image maps of the RPE were used to identify elevated or depressed areas and designate the RPE as one of four types: regular (R), wave (W), band (B), or pond (P) (Fig. 2). Several of these types were defined according to modifications of definitions established in previous studies,[2–4] while others were newly defined. The following objective criteria were used for classification: R-type, no waviness of the boundary between pseudocolors; W-type, waviness of the boundary between pseudocolors; B-type, two outward concavities of the RPE layer and a horizontal ridge

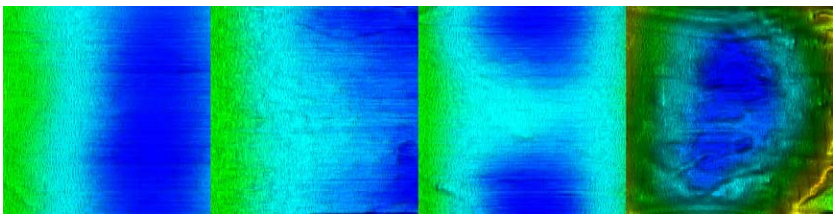

FIGURE 2. Retinal topography types. *Left*: Regular-type. *Middle-left*: Wave-type. *Middle-right*: Band-type. *Right*: Pond-type. The rainbow pseudocolors in the topographic layer image represent height from the coronal plane of the eye, with *blue* indicating low height and *red* indicating high height.

Investigative Ophthalmology & Visual Science

Downloaded from iovs.arvojournals.org on 06/26/2022

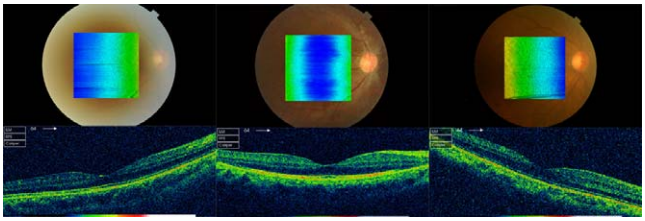

FIGURE 3. Three dimensional characteristics of retinal topography. *Left*: Temporal slope. *Middle*: Middle slope. *Right*: Nasal slope.

between the concavities which are continuous between the fovea and optic disc; and P-type, localized single concavity of the RPE representing a staphyloma. To minimize interpretation bias in classifying RPEs, we processed images using ImageJ software[27] (http://imagej.nih.gov/ij/; provided in the public domain by the National Institutes of Health, Bethesda, MD, USA; Supplementary Fig. S1). Two independent ophthalmologists (IKO, SWK) examined each of the topographies and the interobserver agreement was recorded. The ophthalmologists then met and reviewed the topographies in consensus to arrive at a final classification. When there was disagreement, a third observer (JO) determined the type.

3D Characteristics of Retinal Topography

We characterized RT further according to factors that influenced 3D morphology, such as depression, slope, and central zone topography. To determine the area of greatest depression, we divided the macular area into three zones: the central zone within 1500 μm of the macular center, the superior zone in the superior half of macula minus the central zone, and the inferior zone in the inferior half of the macula minus the central zone. We then identified the zone with greatest area of depression. The slope of the RT was classified as nasal, temporal, or middle slope, which was a modification of previously described methods (Fig. 3).[3] The slope of the RT was determined using differences among pseudocolors at the four corners of the map. A nasal slope was defined as the retina sloping away from the cornea on the nasal side of the eye. When the map was slanted toward the macular center, it was classified as middle slope. We compared the slope of B scan images from 3D volume scanning protocols and line scanning protocols. Central zone topography within 500 μm of the macular center was identified as flat, slanting, or irregular. When categorized into the slanting group, the orientation such as nasal, temporal, inferior, or superior was noted for further analysis.

TABLE 1. Subject Characteristics

	n	Mean ± SD
Age	167	53.3 ± 18.0
Female:male	86:81	
BCVA, logMAR	167	0.10 ± 0.21
ACD, mm	142	3.53 ± 0.35
AL, mm	167	25.87 ± 1.92
Spherical equivalent,* D	167	−4.82 ± 4.80
Refractive astigmatism, D	167	−1.36 ± 1.12
Mean K value, D	143	43.23 ± 2.28
Horizontal K value, D	143	43.06 ± 2.14
Vertical K value, D	143	43.40 ± 3.10
Corneal astigmatism, D	144	−1.28 ± 2.50
Axis difference between refractive astigmatism and corneal astigmatism, deg	142	23.47 ± 21.18

The results are presented as the mean ± SD.
* Spherical equivalent = Sphere + Cylinder/2

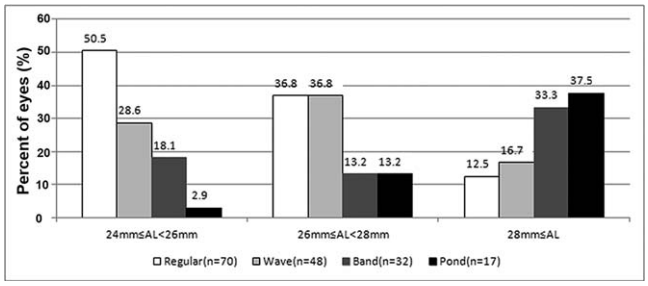

FIGURE 4. Retinal topography and axial length. The distribution of RT type was significantly different among eyes with different degrees of myopia ($P < 0.001$).

Statistical Analysis

Statistical analyses including χ^2 tests and Fisher's exact tests were performed using SPSS software, version 20.0 (SPSS, Inc., Chicago, IL, USA). Results were considered to be statistically significant if the *P* value was less than 0.05. For comparison of optical biometry among RT types, Kruskal-Wallis tests with post hoc analysis were performed.

RESULTS

Subject Characteristics

A total of 167 myopic eyes from 167 subjects met criteria for inclusion in this study (Table 1). The mean age of the 167 subjects was 53.3 ± 18.0 years. Eighty-one (48.5%) subjects were male and 86 (51.5%) were female. There were 116 (69.5%) right eyes and 51 (30.5%) left eyes. The mean refractive error was −4.82 D of spherical equivalent (SE). The mean AL was 25.87 ± 1.92 mm. These ALs were classified into the following three groups based on the distribution of AL: 24 less than or equal to AL less than 26 mm; 26 mm less than or equal to AL less than 28 mm; and AL greater than or equal to 28 mm.

Type of Retinal Topography

Among 167 RTs of myopic eyes, 70 (41.9%) were classified as R-type, 48 (28.7%) as W-type, 32 (19.2%) as B-type, and 17 (10.2%) as P-type. Classification of RT type had a strong interobserver correlation (*kappa* = 0.763, $P < 0.001$). The distribution of RT type was significantly different among eyes with different degrees of AL ($P < 0.001$; Fig. 4). In eyes with a 24 mm less than or equal to AL less than 26 mm, R-type was predominant. However, in eyes with a 26 mm less than or equal AL less than 28 mm, W- and R-types were more frequently observed. P-type was frequently observed in eyes with an AL greater than or equal to 28 mm.

3D Characteristics of Retinal Topography

In 167 RTs from 167 subjects, the area of greatest depression was frequently located in the inferior macula (Table 2). However, it was also located in the superior macula in 17.4% of the eyes studied. Nasal slope was the most commonly observed type of slope in myopic eyes. Temporal slope was more frequently seen than middle slope in eyes with a 26 mm

Investigative Ophthalmology & Visual Science

Downloaded from iovs.arvojournals.org on 06/26/2022

Table 2. Characteristics of Retinal Topography and Axial Length

	Axial length (AL), mm			
	24 ≤ AL < 26, n = 105	26 ≤ AL < 28, n = 38	28 ≤ AL, n = 24	P Value
Area of greatest depression, n = 167				0.028*
Superior, n = 29	24 (22.9%)	4 (10.5%)	1 (4.2%)	
Inferior, n = 81	43 (41.0%)	22 (57.9%)	16 (66.7%)	
Both, n = 45	33 (31.4%)	7 (18.4%)	5 (20.8%)	
Central, n = 12	5 (4.8%)	5 (13.2%)	2 (8.3%)	
Slope, n = 167				0.001†
Nasal, n = 110	78 (74.3%)	20 (52.6%)	12 (50.0%)	
Temporal, n = 30	17 (16.2%)	11 (28.9%)	2 (8.3%)	
Middle, n = 27	10 (9.5%)	7 (18.4%)	10 (41.7%)	
Central zone, n = 166				0.196*
Flat, n = 72	44 (41.9%)	16 (42.1%)	12 (52.2%)	
Slanting, n = 92	61 (58.1%)	21 (55.3%)	10 (43.5%)	
Irregular, n = 2	0 (0%)	1 (2.6%)	1 (4.3%)	

* Fisher's exact test.
† χ^2 test.

less than or equal to AL less than 28 mm. However, middle slope was more frequently observed than temporal slope in eyes with an AL greater than or equal to 28 mm. The slope was not different between of B scan images from 3D volume scanning protocols and line scanning protocols. Topographic characteristics of the central zone of the macula were classified into three subtypes: 72 (43.1%) were flat, 92 (55.1%) were slanted, and 2 (1.2%) were irregular. In the slanted group, the orientation was identified as nasal in 67 eyes (72.8%), temporal in 15 eyes (16.3%), and inferior in 10 eyes (10.9%). None of the retinas studied were oriented in the superior direction. The distribution of topographic characteristics in the central zone of the macula was not different among eyes with different degrees of AL ($P = 0.196$). However, the orientation of slant was significantly different according to the degree of myopia ($P = 0.002$). Nasal orientation was more frequently observed in eyes with an AL less than 26 mm. However, inferior orientation was more frequently observed in eyes with an AL of 28 mm or more.

Each RT type exhibited different 3D characteristics (Table 3). Nasal slope was most frequently observed in R-type eyes. However, temporal slope was not commonly seen in B-type eyes. Middle slope had a tendency to increase from R- to P-type. A slanted central zone of the macula was more frequently observed compared with a flat central zone, except in B-type eyes in which a flat central zone was observed in 87.5% of cases. The area of greatest depression was most frequently located in the inferior macula in all RT types.

Retinal Topography and Optical Measurements

Axial length and SE were different among RT types (Table 4). Difference between refractive astigmatism and corneal astigmatism was also different among RT types. However, axis difference between refractive and corneal astigmatism was not significantly different among RT types. Best-corrected visual acuity (logMAR) was different among types of RT ($P < 0.001$, Kruskal-Wallis test). On post hoc analysis, the AL and SE of P-type RT were greater than that of R-type (Table 5). Difference between refractive and corneal astigmatism of P-type RT was greater than that of B-type ($P = 0.002$). Best-corrected visual acuity of P-type was worse than R-, W-, or B-type ($P < 0.001$, $P = 0.007$, and $P < 0.001$, respectively).

Table 3. Three Dimensional Characteristics of Retinal Topography Types

	Type				
	Regular, n = 70	Wave, n = 48	Band, n = 32	Pond, n = 17	P Value*
Area of greatest depression					<0.001
Superior, n = 29	13 (18.6%)	8 (16.7%)	8 (25.0%)	0 (0%)	
Inferior, n = 81	23 (32.9%)	31 (64.6%)	13 (40.6%)	14 (82.4%)	
Both, n = 45	27 (38.6%)	7 (14.6%)	11 (34.4%)	0 (0%)	
Central, n = 12	7 (10.0%)	2 (4.2%)	0 (0%)	3 (17.6%)	
Slope					<0.001
Nasal, n = 110	52 (74.3%)	31 (64.6%)	23 (71.9%)	4 (23.5%)	
Temporal, n = 30	16 (22.9%)	12 (25.0%)	1 (3.1%)	1 (5.9%)	
Middle, n = 27	2 (2.9%)	5 (10.4%)	8 (25.0%)	12 (70.6%)	
Central zone					<0.001
Flat, n = 72	25 (35.7%)	15 (31.3%)	28 (87.5%)	4 (25.0%)	
Slanting, n = 92	45 (64.3%)	32 (66.7%)	4 (12.5%)	11 (68.8%)	
Irregular, n = 2	0 (0%)	1 (2.1%)	0 (0%)	1 (6.3%)	

* Fisher's exact test.

Discussion

In this study, we determined RT of the macula using an SD-OCT volume scan in eyes with varying degrees of myopia. Although the 2- and 3D curvature of the RPE layer has previously been reported in emmetropic or highly myopic eyes,[3,4,28–30] this is the first study to investigate 3D RT in eyes with varying degrees of myopia. In a previous study, which used horizontal scans, the inward convexity may be less clearly detected.[31] In this study using a pseudocolor coded topographic image map of the RPE from 3D-OCT scans, we were able to easily identify B-type RT in eyes with all degrees of myopia. The rainbow pseudocolors in the topographic layer image represent height from the coronal plane of the eye, with blue indicating low height and red indicating high height. This could be used as an objective tool to depict the 3D configuration of the RPE. Using this method, we were able to examine the shape of the photoreceptor array in situ. The topographic images for RPEs on Topcon 3D-OCT are recognized as segmentation images of the top of the RPE layer, which corresponds to the outer segment tips of the photoreceptors.[32] Thus, RT images in this study may provide realistic measurements of the retinal photoreceptor array. However, the topographic images of the RPE layers are provided not only by the 3D-OCT but also by other SD-OCTs. Since the photoreceptor layers are usually arrayed with RPE layers, topographic maps for the RPE layers generated by other SD-OCTs may be useful alternatives for observing the topographic characteristics.

We found that the distribution of RT type differs according to the degree of AL. In eyes with a low degree of AL, 50.5%

Investigative Ophthalmology & Visual Science

Downloaded from iovs.arvojournals.org on 06/26/2022

Table 4. Comparison of Biometric Characteristics Among Various Types of Retinal Topography

	Type				
	Regular, $n = 70$	Wave, $n = 48$	Band, $n = 32$	Pond, $n = 17$	*P* Value*
AL, mm	24.69 (24.36, 25.58)	25.12 (24.39, 27.07)	24.92 (24.28, 27.68)	28.03 (26.34, 30.16)	<0.001
Refractive error					
SE,† D	−2.63 (−5.31, −0.88)	−2.50 (−9.00, −1.00)	−3.88 (−8.31, −0.88)	−7.63 (−11.59, −3.31)	0.006
Cylinder, D	−1.13 (−1.75, −0.50)	−1.25 (−1.75, −0.75)	−1.00 (−1.50, −0.50)	−1.75 (−3.88, −0.75)	0.092
Axis, deg	80.5 (25.5, 113.3)	82.0 (56.0, 141.0)	101.0 (76.0, 143.0)	76.0 (27.8, 155.3)	0.160
Mean K, D	43.36 (42.37, 45.07)	42.89 (42.01, 44.29)	43.44 (42.62, 44.35)	43.51 (40.64, 45.58)	0.636
Difference between refractive astigmatism and corneal astigmatism, D	0.56 (0.33, 0.98)	0.48 (0.26, 0.85)	0.39 (0.21, 0.74)	1.15 (0.44, 1.67)	0.008
Axis difference between refractive astigmatism and corneal astigmatism, deg	21.0 (7.8, 38.3)	11.0 (5.0, 31.0)	13.0 (5.5, 37.5)	11.5 (4.5, 31.5)	0.573
BCVA, logMAR	0.000 (0.000, 0.046)	0.000 (0.000, 0.155)	0.000 (0.000, 0.023)	0.188 (0.024, 0.301)	0.001

Results are presented as the median (interquartile range).
* *P* value: Kruskal-Wallis test.
† Spherical equivalent = Sphere + Cylinder/2.

exhibited R-type topography. However, as the degree of AL increased, fewer exhibited R-type and a greater proportion were found to be W or B-type. In eyes with a high degree of AL, 37.5% were P-type. These results support the previous suggestion that the posterior curvature of the eye changes with progression of myopia.[33] Ohno-Matsui and associates[3] previously hypothesized that progression of eye deformities in myopic eyes occurs due to changes in the curvature of the inner scleral surface and Bruch's membrane. They also suggested that the posterior sclera may expand when a posterior staphyloma develops later in life. Other studies have shown that the bulge in eyes with a dome-shaped macula may prevent schisis or detachment, and also act as a compensatory mechanism during ocular development.[34] We defined B-type as having a dome-shaped macula or band-shaped ridge.[28,29] B-type topography was observed in eyes with all degrees of myopia in our study. This suggests that while B-type topography may be present in myopic eyes of varying degrees, it is potentially enhanced with progression of myopia. This may also mean that B-type RT is not simply a consequence of staphyloma, but may also be an early indicator of the development of staphyloma. In this study, we newly defined W-type RT, which is similar to B-type without the horizontal ridge, which continues between the fovea and optic disc. Both types can exhibit outward concavities of the RPE. However, B-type may be the more advanced form of W-type, since W-type was more frequently observed in eyes with low- and medium-grade myopia. In our study of eyes with varying degrees of AL, R-type topography was predominantly seen in cases of low grade myopia, W-type in moderate myopia, and B- or P-type in high myopia. While our results suggest that changes in RT type occur with progression of myopia, additional prospective studies are needed with long term observation to confirm our findings.

Table 5. Post Hoc Analysis

	P Value		
	Axial Length	Spherical Equivalent	Difference Between Refractive Astigmatism and Corneal Astigmatism, D
Regular type vs. wave type	0.081	0.238	0.990
Regular type vs. band type	0.208	0.064	0.036
Regular type vs. pond type	<0.001*	0.001*	0.027
Wave type vs. band type	0.922	0.520	0.267
Wave type vs. pond type	<0.001*	0.018	0.013
Band type vs. pond type	0.004*	0.048	0.002*

* Significant by Mann-Whitney *U* test using Bonferroni's correction for multiple comparisons.

We characterized RT using several factors such as the area of greatest depression, slope, and central zone topography. On 3D segmentation maps, 81 (48.5%) of 167 eyes exhibited an area of greatest depression in the inferior area, and only 12 (7.2%) of 167 eyes showed this within the visual axis. These results differ from those of a previous study that used 2D line scan in eyes with high myopia, in which 21.7% of eyes had an area of greatest depression below the visual axis.[2] We also found that 29 (17.4%) of 167 eyes had an area of greatest depression in the superior portion of the macula, compared with 0 cases reported in the previous study.[2] These differences may be due to varying degrees of myopia or the use of different methods to determine the area of greatest depression. In the current study, the most depressed area was determined using 3D maps of the RPE layer. The distribution varied according to AL. In 22.9% of eyes with an AL less than 26 mm, the area of greatest depression was in the superior portion of the macula. However, this was only true in 4.2% to 10.5% of eyes with an AL greater than 26 mm. The proportion of eyes with the most depressed area in the inferior macula was greater in eyes with a longer AL. This may be because the lower one-half of the eye is structurally weaker since the optic fissure develops on the ventral side of the optic cup during formation of the eye.[35] In a previous study that used 2D scan images, the curvature of the RPE was classified into two types: straight contour that sloped toward the optic disc or roughly symmetrical curvature centered on the fovea.[3] In our study, we classified the slope into three types, each of which were representative of the curvature. Nasal slope was the predominant type observed in all degrees of myopia. Temporal and middle slope were more frequently observed in eyes with moderate to high myopia.

Investigative Ophthalmology & Visual Science

Downloaded from iovs.arvojournals.org on 06/26/2022

The macular center is the region in which cone cells are highly concentrated, and is known to be important for fine vision. Photoreceptors are regularly arrayed in the visual axis to maximize the ability to receive photons passing through the eye.[10,11] In this study, the symmetry around the foveal center was considered in the classification of central zone configuration. In myopic eyes, the topography of the central zone was more frequently slanted. However, in eyes with B-type RT, it was more frequently flat. This suggests that B-type RT sustains the array of photoreceptors in the visual axis.

In this study, P-type RT had lower BCVA than the other three types. However, the BCVA of the W- and B-types, which had similar topographic characteristics to those of R-type, was not different from R-type. Difference between refractive astigmatism and corneal astigmatism was different among RT types. We found that difference between refractive astigmatism and corneal astigmatism was different among RT types. Retinal topography may be related with the optical characteristics of the eye. The optical characteristics of the eye can be determined according to the features of its components, including the cornea, pupil, crystalline lens, and retina.[36] Each photoreceptor functions as a "light pipe," or a fiber optic, which is directed to the second nodal point of the eye.[11,36] This orientation optimally receives light and forms an image.[36,37] Since myopic eyes were often found to exhibit irregular topography, there may be concurrent suboptimal orientation of photoreceptors contributing to visual deterioration. In addition to corneal, pupillary, and lens factors, ocular aberration measurements could be influenced by retinal factors and the array of photoreceptors, which is dependent on the 3D configuration of the choroid and the sclera.[38,39] However, it is difficult to measure retinal factors that influence ocular aberration. In this retrospective study, we did not measured higher-order aberrations. However, we present methods of measuring RT using commercially available SD-OCT. This technique could be used to monitor retinal factors influencing ocular aberration and vision. Additional prospective studies that use an aberrometer and SD-OCT could help to further establish the impact of retinal aberration on ocular aberration in eyes with retinal disease.

Previously, staphylomas were classified into several subtypes.[1] However, in this study, we were unable to classify staphylomas using macular OCT. Only a localized portion of the macula was the focus of this study. Although this study covered a limited area, the results were obtained based on images that included the macular area using 3D volume scans with compact B-scans. While we used images that covered a 6 mm $\times$ 6 mm area of the macula that is likely important for fine vision, the myopic change in RT occurs in the entirety of the eye. Thus, use of a smaller defined area may limit our understanding of these changes. This study was limited by the small sample size included in each group as well as by the retrospective design. Additionally, we included myopic eyes, but not eyes with other macular diseases. The classification of RT types as seen on pseudocolor topographic maps into discrete groups is an arbitrary designation, since the range of topographic types in a population of myopic retinas is part of a continuum. In this study, we determined the topographic type using an imaging program, and obtained a high degree of reproducibility. Although we did not find the difference in the slope between images from 3D-volume scanning protocols and line scanning protocols, an alignment between an eye and OCT at the time of image acquisition may influence the result regarding the slope and central zone topography. Finally, while this was a cross-sectional study, longitudinal studies using a more advanced scan protocol that covers a wider area may be useful in overcoming these limitations.

In conclusion, RT representing the outer retinal boundary varied with the degree of AL. The difference of RT characteristics may be originated from the difference between healthy eyes and highly myopic eyes. And the differences may be related with optical biometry of myopic eyes. Retinal tomography using SD-OCT might be useful for monitoring morphologic changes of the retina with respect to progression of myopia.

Acknowledgments

This study was presented in part at the 109th Annual Meeting of The Korean Ophthalmological Society in Seoul, Korea, April 2013.

Supported by a grant from the Korean Health Technology R&D Project, Ministry for Health, Welfare & Family Affairs, Republic of Korea (HI10C1979; Sejong, Korea).

Disclosure: **I.K. Oh**, None; **J. Oh**, None; **K.-S. Yang**, None; **K.H. Lee**, None; **S.-W. Kim**, None; **K. Huh**, None

References

1. Curtin BJ. The posterior staphyloma of pathologic myopia. *Trans Am Ophthalmol Soc*. 1977;75:67–86.
2. Moriyama M, Ohno-Matsui K, Hayashi K, et al. Topographic analyses of shape of eyes with pathologic myopia by high-resolution three-dimensional magnetic resonance imaging. *Ophthalmology*. 2011;118:1626–1637.
3. Ohno-Matsui K, Akiba M, Modegi T, et al. Association between shape of sclera and myopic retinochoroidal lesions in patients with pathologic myopia. *Invest Ophthalmol Vis Sci*. 2012;53:6046–6061.
4. Gaucher D, Erginay A, Lecleire-Collet A, et al. Dome-shaped macula in eyes with myopic posterior staphyloma. *Am J Ophthalmol*. 2008;145:909–914.
5. Agte S, Junek S, Matthias S, et al. A. Müller glial cell-provided cellular light guidance through the vital guinea-pig retina. *Biophys J*. 2011;101:2611–2619.
6. Wade NJ. Image, eye, and retina (invited review). *J Opt Soc Am A Opt Image Sci Vis*. 2007;24:1229–1249.
7. DelMonte DW, Anatomy Kim T. and physiology of the cornea. *J Cataract Refract Surg*. 2011;37:588–598.
8. Labin AM, Ribak EN. Retinal glial cells enhance human vision acuity. *Phys Rev Lett*. 2010;104:158102.
9. Willbold E, Layer PG. Müller glia cells and their possible roles during retina differentiation in vivo and in vitro. *Histol Histopathol*. 1998;13:531–552.
10. Franze K, Grosche J, Skatchkov SN, et al. Müller cells are living optical fibers in the vertebrate retina. *Proc Natl Acad Sci U S A*. 2007;104:8287–8292.
11. Solovei I, Kreysing M, Lanctôt C, et al. Nuclear architecture of rod photoreceptor cells adapts to vision in mammalian evolution. *Cell*. 2009;137:356–368.
12. Ragoczy T, Groudine M. The nucleus inside out through a rod darkly. *Cell*. 2009;137:205–207.
13. Reichenbach A, Bringmann A. *Muller Cells in the Healthy and Diseased Retina*. New York: Springer; 2010.
14. Westheimer G. Directional sensitivity of the retina: 75 years of Stiles-Crawford effect. *Proc Biol Sci*. 2008;275:2777–2786.
15. Snyder AW, Pask C. The Stiles-Crawford effect–explanation and consequences. *Vision Res*. 1973;13:1115–1137.
16. Bae SW, Chae JB. Assessment of metamorphopsia in patients with central serous chorioretinopathy. *Indian J Ophthalmol*. 2013;61:172–175.
17. Costa VP, Arcieri ES. Hypotony maculopathy. *Acta Ophthalmol Scand*. 2007;85:586–597.

Downloaded from iovs.arvojournals.org on 06/26/2022

18. Arimura E, Matsumoto C, Okuyama S, Takada S, Hashimoto S, Shimomura Y. Retinal contraction and metamorphopsia scores in eyes with idiopathic epiretinal membrane. *Invest Ophthalmol Vis Sci*. 2005;46:2961–2966.
19. Gregori G, Wang F, Rosenfeld PJ, et al. Spectral domain optical coherence tomography imaging of drusen in nonexudative age-related macular degeneration. *Ophthalmology*. 2011;118: 1373–1379.
20. Ortiz S, Siedlecki D, Pérez-Merino P, et al. Corneal topography from spectral optical coherence tomography (sOCT). *Biomed Opt Express*. 2011;2:3232–3247.
21. Ambrósio R Jr, Belin MW. Imaging of the cornea: topography vs tomography. *J Refract Surg*. 2010;26:847–849.
22. Dingeldein SA, Klyce SD. The topography of normal corneas. *Arch Ophthalmol*. 1989;107:512–518.
23. Bogan SJ, Waring GO III, Ibrahim O, Drews C, Curtis L. Classification of normal corneal topography based on computer-assisted videokeratography. *Arch Ophthalmol*. 1990; 108:945–949.
24. Rosales P, Marcos S. Pentacam Scheimpflug quantitative imaging of the crystalline lens and intraocular lens. *J Refract Surg*. 2009;25:421–428.
25. Oh JH, Oh J, Togloom A, Kim SW, Huh K. Biometric characteristics of eyes with central serous chorioretinopathy. *Invest Ophthalmol Vis Sci*. 2014;55:1502–1508.
26. Liu Z, Huang AJ, Pflugfelder SC. Evaluation of corneal thickness and topography in normal eyes using the Orbscan corneal topography system. *Br J Ophthalmol*. 1999;83:774–778.
27. Rasband W. Image J medical imaging software. Bethesda, MD: National Institutes of Health. Available at: Available at: http://rsb.info.nih.gov/ij/. Accessed July 1, 2013.
28. Imamura Y, Iida T, Maruko I, Zweifel SA, Spaide RF. Enhanced depth imaging optical coherence tomography of the sclera in dome-shaped macula. *Am J Ophthalmol*. 2011;151:297–302.
29. Ellabban AA, Tsujikawa A, Matsumoto A, et al. Three-dimensional tomographic features of dome-shaped macula by swept-source optical coherence tomography. *Am J Ophthalmol*. 2013;155:320–328, e2.
30. Caillaux V, Gaucher D, Gualino V, Massin P, Tadayoni R, Gaudric A. Morphologic characterization of dome-shaped macula in myopic eyes with serous macular detachment. *Am J Ophthalmol*. 2013;156:958–967.
31. Coco RM, Sanabria MR, Alegría J. Pathology associated with optical coherence tomography macular bending due to either dome-shaped macula or inferior staphyloma in myopic patients. *Ophthalmologica*. 2012;228:7–12.
32. Sayanagi K, Sharma S, Kaiser PK. Comparison of retinal thickness measurements between three-dimensional and radial scans on spectral-domain optical coherence tomography. *Am J Ophthalmol*. 2009;148:431–438.
33. Moriyama M, Ohno-Matsui K, Modegi T, et al. Quantitative analysis of high-resolution 3D MR images of highly myopic eyes to determine their shapes. *Invest Ophthalmol Vis Sci*. 2012;53:4510–4518.
34. Keane PA, Mitra A, Khan IJ, Quhill F, Elsherbiny SM. Dome-shaped macula: a compensatory mechanism in myopic anisometropia? *Ophthalmic Surg Lasers Imaging*. 2012;43: e52–e54.
35. Moore KL, Persaud TVN. The eye and ear, 5th ed. In: KL, Moore, Persaud TVN, eds. *The Developing Human-Clinically Oriented Embryology*. Philadelphia, PA: WB Saunders; 1993: 423–432.
36. Miller D, Schor P, Magnante P. Optics of the normal eye, 3rd ed. In: Yanoff M, Duker JS, eds. *Ophthalmology*. Philadelphia, PA: Mosby; 2008:52–60.
37. Enoch JM. Vertebrate rod receptors are directionally sensitive. In: Snyder AW, Menzel R, eds. *Photoreceptor Optics*. Berlin, Germany: Springer-Verlag; 1975:17–37.
38. Zarei-Ghanavati S, Banaee T, Abrishami M, Dehghani A. Macular disease affects the outcome of ZyWave aberrometry. *Ophthalmic Surg Lasers Imaging*. 2011;42:26–30.
39. Bessho K, Bartsch DU, Gomez L, Cheng L, Koh HJ, Freeman WR. Ocular wavefront aberrations in patients with macular diseases. *Retina*. 2009;29:1356–1363.

Investigative Ophthalmology & Visual Science

Downloaded from iovs.arvojournals.org on 06/26/2022